Peer-Reviewed Technical Communication

Robust Multitarget Tracking in Forward-Looking Sonar Image Sequences Using Navigational Data

Isabelle Quidu, Luc Jaulin, Alain Bertholom, and Yann Dupas

***Abstract*—This paper presents a new approach to the problem of tracking objects in sequences of forward-looking sonar images. Unlike previous work, navigational data are taken as inputs to the state model of the Kalman filter used for tracking fixed obstacles. This model allows a robust prediction of their apparent motion in relation to the position of the sonar. A complete framework is presented where detection and data association issues are also discussed. An assessment of the proposed method has been carried out on real data from two different systems. Moreover, whereas the state model was first derived for a ground obstacle, a modified state model is proposed to estimate the altitude of the obstacle in relation to the sonar position using a number of successive pings.**

***Index Terms*—Autonomous underwater vehicles (AUVs), multitarget tracking, obstacle avoidance, process modeling.**

I. Introduction

AUTONOMOUS UNDERWATER VEHICLES (AUVs) are expected to perform survey missions in both known and unknown environments. While the primary mission of an AUV is usually data collection, generally achieved by means of a sidescan sonar or multibeam echosounder, another key task is to ensure its safety. For this, the AUV can be equipped with a forward-looking sonar (FLS) by which it is able to sense the environment at a certain distance in the direction of travel. The main objective is to determine whether it is faced with an obstacle, to avoid a collision that could damage the vehicle. After an initial detection, the AUV first has to track the object to confirm the existence of an obstacle and obtain information about it. This must be done sufficiently early, i.e., at a safe distance between the AUV and the obstacle, to perform an avoidance maneuver if necessary.

This paper focuses on the tracking of multiple fixed objects through a sequence of FLS images. Robustness relies on the integration in the process of accurate navigational data obtained via an iXSea (iXBlue company, Marly Le Roi, France) Inertial Navigation Unit (INU) and an RD Instruments (RDI; Poway, CA) Doppler velocity log (DVL).

In previous work dealing with FLS data, object-based tracking between successive frames is generally based solely on the incoming sonar data. In addition, most of them focus on moving obstacles, although Williams *et al.* developed a Kalman filter for the localization of stationary obstacle between successive frames [1]. In a broad sense, an object appears to be moving due to either platform motion (the present case) or its own movement (the more general case). Cobb *et al.* proposed a low-power tracking and homing algorithm for a stationary floating object [2]. Lane *et al.* performed optical flow calculations on moving objects and used the motion estimates to match them with new returns (i.e., object detections) with a metric called the compatibility value [3]. A tracking tree then allows keeping several possible tracks for a deferred decision. More recently, Trucco *et al.* followed by Petillot *et al.* used Kalman filters as the core element of their tracking schemes with an extended state vector composed of position and area and their associated first and second derivatives [4], [5]. Clark *et al.* then compared this traditional approach including a Kalman filter for each target and a nearest neighbor algorithm for data association with a new approach using the developed particle implementation of the multiple-target probability hypothesis density (PHD) filter proposed by Mahler and a target state estimate-to-track data association technique [6], [7]. Finally, a multitarget tracking method using a Dual frequency Identification SONar (DIDSON) sonar to monitor fish movement in trawls was presented in [8]. Tracking is performed by a simple alpha–beta fixed gain filter and a global nearest neighbor method [9].

In this paper, we aim to perform real-time tracking by means of Kalman filtering that takes navigational data as inputs. Section II describes the detector algorithm that provides measurements for track initiation and update. Unlike previous work, a new state model, described in Section III, has been derived from the AUV process model. This allows the prediction of the polar coordinates of an obstacle under the assumptions that the obstacle is fixed and lies on the seabed. This process model

Manuscript received February 21, 2011; revised November 15, 2011; accepted March 05, 2012. Date of publication May 16, 2012; date of current version July 10, 2012. This work was supported by the Groupe d'Etudes Sous-Marines de l'Atlantique (GESMA), a division of the French Ministry of Defense (DGA).

Associate Editor: D. A. Abraham.

I. Quidu and L. Jaulin are with the Lab-STICC UMR CNRS 6285, Ecole Nationale de Techniques Avancées (ENSTA) Bretagne, Brest Cedex 9 29806, France (e-mail: isabelle.quidu@ensta-bretagne.fr; luc.jaulin@ensta-bretagne.fr).

A. Bertholom is with the Groupe d'Etudes Sous-Marines de l'Atlantique (GESMA), DGA/DET/GESMA, Brest Armées 29240, France (e-mail: alain.bertholom@dga.defense.gouv.fr).

Y. Dupas is with the Service Hydrographique et Océanographique de la Marine (SHOM), SHOM/DO/HOM/DEV, Brest 29200, France (e-mail: yann.dupas@shom.fr).

Color versions of one or more of the figures in this paper are available online at http://ieeexplore.ieee.org.

This paper has supplementary downloadable materials available at http://ieeexplore.ieee.org., provided by the author. Contact isabelle.quidu@ensta-bretagne.fr for further questions about this work.

Digital Object Identifier 10.1109/JOE.2012.2190572

TABLE I
GENERAL PARAMETERS

General parameters	
$\boldsymbol{x}=(d \quad \delta)^T$	Polar coordinates (meters, radians) of the target in the sonar frame
$\boldsymbol{y}=(y^i \quad y^j)^T$	Screen coordinates of the target in pixels
Δd	Along-track sampling rate in meters
$\Delta\delta$	Across-track sampling rate in degrees
$\boldsymbol{p_a}=(p_a^x \quad p_a^y \quad p_a^z)^T$	Coordinate vector of the AUV in the world reference frame in meters
$\boldsymbol{m_a}=(m_a^x \quad m_a^y \quad m_a^z)^T$	Coordinate vector of a proud seafloor object in the world reference frame in meters
$\boldsymbol{p_r}=(p_r^x \quad p_r^y \quad p_r^z)^T$	Coordinate vector of the AUV in the relative reference frame in meters
$\boldsymbol{m_r}=(m_r^x \quad m_r^y \quad m_r^z)^T$	Coordinate vector of a proud seafloor object in the relative reference frame in meters
$\boldsymbol{V}_a=(v_a^x \quad v_a^y \quad v_a^z)^T$	Velocity vector of the AUV in the world reference frame in meters per second
$\boldsymbol{V}_r=(v_r^x \quad v_r^y \quad v_r^z)^T$	Velocity vector of the AUV in the relative reference frame in meters per second
h	AUV altitude in meters
d_{st}	Distance between the sonar and the target along the z-axis
(φ,θ,ψ)	Euler angles[1] (roll, pitch, yaw) in radians
R_ψ	Yaw rotation matrix
R_θ	Pitch rotation matrix
R_φ	Roll rotation matrix
$R_{euler}(\varphi,\theta,\psi)$	Euler rotation matrix, *i.e.* three composed rotations $R_\psi, R_\theta, R_\varphi$ that move the relative reference frame to the world reference frame. Its arguments are the Euler angles.
$f_a,\ f_b,\ f_c$	Intermediate functions involved in the process modeling
f	Process model function
c_v	Coefficient of variation

[1] The Euler angles are three angles introduced by Euler (1770) to describe the orientation of a rigid body or equivalently a rotation matrix. To describe such an orientation three parameters are required. These parameters make possible to describe a motion from a reference frame to a given referred frame. This motion can be described in various ways. One of them, called the ZYX or Yaw-Pitch-Roll formulation, is commonly used in underwater robotics.

is the state model of a Kalman filter described in Section IV and navigational data are used as inputs so as to allow robust tracking of an obstacle even if the vehicle changes its velocity and/or its attitude. In Section V, data association is performed to take advantage of the behavior of the Kalman filter via the innovation term. According to the assumed condition of a seafloor object, tracking of a tethered object in the water column is not performed especially well. To address this, a "batch" procedure which requires some number of consecutive pings to function has been proposed: it performs a deferred estimation of the tether length by minimizing the innovation value through the tracking procedure. This procedure is explained in Section VI. Section VII gives several results on real data obtained by two different FLS, after which some concluding remarks are made in Section VIII.

Notations for the main parameters used in this paper are listed in Tables I and II. Some parameters are to be used in the world (absolute) reference frame (O_a, $\boldsymbol{x_a}$, $\boldsymbol{y_a}$, $\boldsymbol{z_a}$) (O_a: center of gravity of Earth, $\boldsymbol{x_a}$: geographical north direction, $\boldsymbol{y_a}$: east direction, $\boldsymbol{z_a}$: gravity direction) on the one hand, and in the relative reference frame (O_r, $\boldsymbol{x_r}$, $\boldsymbol{y_r}$, $\boldsymbol{z_r}$) (O_r: center of gravity of the vehicle, $\boldsymbol{x_r}$: the direction of movement of the vehicle, $\boldsymbol{y_r}$: toward its right, $\boldsymbol{z_r}$: down) on the other hand.

II. OBJECT DETECTION

To track an obstacle in a series of sonar images, it must first be discriminated from the background signal by employing some kind of a detection algorithm. In imaging sonar, detection is sometimes performed by segmentation and can be achieved by a double thresholding (one for echoes from the object, one for the acoustic shadows cast on the seafloor) with or without prefiltering the image [5], [10].

Here, a simple goodness-of-fit test is performed to detect statistical deviations from which detected points can be derived. This test exploits the fact that high-frequency sonar images suffer from a well-known multiplicative noise process that is commonly called the *speckle* [11], [12].

When the number of scatterers in a resolution cell is sufficiently high, the pixel gray levels follow a Rayleigh law. Under this hypothesis, we have derived a simple goodness-of-fit test that consists in verifying the ratio value between the mean and the standard deviation of pixels, called the coefficient of variation c_v [13]. This coefficient is constant for a Rayleigh-distributed variable and equal to

$$c_v^{\text{th}} = \sqrt{\frac{4}{\pi} - 1} = 0.52. \tag{1}$$

TABLE II
KALMAN FILTER PARAMETERS

Kalman filter parameters	
k	Step number
$\boldsymbol{x}_k$	State vector at step k
$\boldsymbol{x}_{k\|k-1}$	State vector at step k given data from step k-1
$\boldsymbol{y}_k$	Measurement vector at step k
$\boldsymbol{u}_k$	Input vector at step k
$\boldsymbol{v}_k$	Gaussian state noise at step k
$\boldsymbol{w}_k$	Gaussian measurement noise at step k
Q_k	Noise covariance matrix at step k
R_k	Measurement covariance matrix at step k
d_R	Scaling scalar in meters for R_k
P_k	State covariance matrix at step k
$\boldsymbol{v}_k = \boldsymbol{y}_k - \hat{\boldsymbol{y}}_{k/k-1}$	Innovation term at step k
R_k^v	Innovation covariance matrix at step k
$\boldsymbol{\chi}_k^i$	Sigma point number i for unscented Kalman filtering at step k
W_i	Weight parameter of the Sigma point number i for unscented Kalman filtering

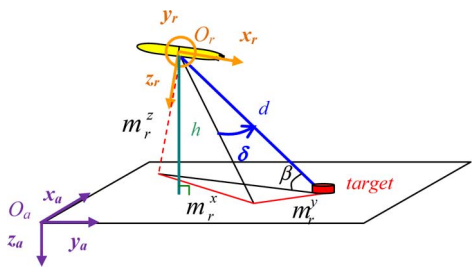

Fig. 1. Operational configuration (O_a supposed to be the center of gravity of Earth).

The practical implementation of this test is given in Section VII-B.

The simple ratio test above has been compared to the nonparametric Kolmogorov–Smirnov statistical test for equal distributions, which gives similar results but requires a higher computation time.

III. PROCESS MODEL

To use the Kalman filter to track obstacles given noisy detection points, we first have to define the state model. This is the process model that provides the sonar coordinates (d, δ), i.e., the polar coordinates (meters, radians) of the target in the sonar frame, of a detected object given the AUV motion [15]. It is obtained as follows.

In the relative reference frame, a seafloor target is located by means of the following equations (see Fig. 1):

$$\begin{cases} (m_r^x)^2 + (m_r^y)^2 + (m_r^z)^2 = d^2 \\ m_r^y = d\sin(\delta) \\ -\sin(\theta)\, m_r^x + \cos(\theta)\sin(\varphi)\, m_r^y + \cos(\theta)\cos(\varphi)\, m_r^z = h \end{cases} \tag{2}$$

where $\boldsymbol{m_r} = (m_r^x\ m_r^y\ m_r^z)^T$ is the coordinate vector of the proud seafloor target, h is the AUV altitude in meters, and (φ, θ, ψ) are the Euler angles that define the attitude of the vehicle.

From these equations, it can be shown that $a_1 (m_r^x)^2 + b_1 m_r^x + c_1 = 0$, when

$$a_1 = \left[1 + \left[\frac{\sin(\theta)}{\cos(\theta)\cos(\varphi)}\right]^2\right]$$

$$b_1 = 2\frac{\sin(\theta)}{\cos^2(\theta)\cos^2(\varphi)}[h - d\cos(\theta)\sin(\varphi)\sin(\delta)]$$

$$c_1 = d^2[\sin^2(\delta) - 1] + \left[\frac{h - d\cos(\theta)\sin(\varphi)\sin(\delta)}{\cos(\theta)\cos(\varphi)}\right]^2$$

so that

$$\begin{pmatrix} m_r^x \\ m_r^y \\ m_r^z \end{pmatrix} = \begin{pmatrix} \dfrac{-b_1 + \sqrt{\Delta_1}}{2a_1} \\ d\sin(\delta) \\ \dfrac{h + \sin(\theta)\left(\frac{-b_1+\sqrt{\Delta_1}}{2a_1}\right) - d\cos(\theta)\sin(\varphi)\sin(\delta)}{\cos(\theta)\cos(\varphi)} \end{pmatrix}$$

where $\Delta_1 = b_1^2 - 4a_1c_1$. That is

$$\begin{pmatrix} m_r^x \\ m_r^y \\ m_r^z \end{pmatrix} = f_a(d, \delta). \tag{3}$$

Let $(\dot{d}, \dot{\delta}) = (\partial d/\partial t, \partial \delta/\partial t)$ be the derivative of the state vector with respect to time. It can be derived from the two first equations of (2), such that

$$\dot{d} = \frac{\dot{m}_r^x m_r^x + \dot{m}_r^y m_r^y + \dot{m}_r^z m_r^z}{d}$$
$$\dot{\delta} = \frac{\dot{m}_r^y - \frac{\sin(\delta)}{d}\left(\dot{m}_r^x m_r^x + \dot{m}_r^y m_r^y + \dot{m}_r^z m_r^z\right)}{d\cos(\delta)},$$
$$\text{i.e.,} (\dot{d}, \dot{\delta}) = f_c\left(\dot{m}_r^x, \dot{m}_r^y, \dot{m}_r^z, d, \delta\right). \quad (4)$$

By introducing the Euler rotation matrix R_{euler} defined as

$$R_{\text{euler}}(\varphi, \theta, \psi) = R_\psi R_\theta R_\varphi = \begin{pmatrix} \cos(\psi) & -\sin(\psi) & 0 \\ \sin(\psi) & \cos(\psi) & 0 \\ 0 & 0 & 1 \end{pmatrix} \times \begin{pmatrix} \cos(\theta) & 0 & \sin(\theta) \\ 0 & 1 & 0 \\ -\sin(\theta) & 0 & \cos(\theta) \end{pmatrix} \begin{pmatrix} 1 & 0 & 0 \\ 0 & \cos(\varphi) & -\sin(\varphi) \\ 0 & \sin(\varphi) & \cos(\varphi) \end{pmatrix}$$

we can write

$$\boldsymbol{p_a} - \boldsymbol{m_a} = -R_{\text{euler}}(\varphi, \theta, \psi) \cdot \boldsymbol{m_r} \quad (5)$$

where $\boldsymbol{p_a} = (p_a^x \quad p_a^y \quad p_a^z)^T$ is the coordinate vector of the AUV in the world reference frame in meters (we assume that its location is coincident with all the other sensors) and $\boldsymbol{m_a} = (m_a^x \quad m_a^y \quad m_a^z)^T$ is the coordinate vector of the proud seafloor object in the world reference frame in meters. Also, the Euler angles (φ, θ, ψ) for roll, pitch, and yaw are defined in radians.

By differentiating (5), we obtain

$$\boldsymbol{V_a} = -\dot{R}_{\text{euler}} \cdot \boldsymbol{m_r} - R_{\text{euler}} \cdot \dot{\boldsymbol{m}}_{\boldsymbol{r}}$$

with $\boldsymbol{V_a} = R_{\text{euler}}(\varphi, \theta, \psi) \cdot \boldsymbol{V_r}$ being the velocity of the AUV in the world reference frame in meters per second, so that

$$\dot{\boldsymbol{m}}_{\boldsymbol{r}} = -R_{\text{euler}}^T(\varphi, \theta, \psi)\dot{R}_{\text{euler}}(\dot{\varphi}, \dot{\theta}, \dot{\psi})\boldsymbol{m_r} - \boldsymbol{V}_r,$$
$$= f_b\left(m_r^x, m_r^y, m_r^z, \boldsymbol{V_r}, \varphi, \theta, \psi, \dot{\varphi}, \dot{\theta}, \dot{\psi}\right) \quad (6)$$

by exploiting the unitary nature of the Euler matrix and where $\boldsymbol{V}_r = (v_r^x \quad v_r^y \quad v_r^z)^T$ is the velocity vector of the AUV in the relative reference frame, and $\dot{R}_{\text{euler}}(\varphi, \theta, \psi, \dot{\varphi}, \dot{\theta}, \dot{\psi})$ is defined as

$$\dot{R}_{\text{euler}}(\varphi, \theta, \psi, \dot{\varphi}, \dot{\theta}, \dot{\psi}) = \dot{\psi}\begin{pmatrix} 0 & -1 & 0 \\ 1 & 0 & 0 \\ 0 & 0 & 0 \end{pmatrix} R_\psi R_\theta R_\varphi + \dot{\theta} R_\psi \times \begin{pmatrix} 0 & 0 & 1 \\ 0 & 0 & 0 \\ -1 & 0 & 0 \end{pmatrix} R_\theta R_\varphi + \dot{\varphi} R_\psi R_\theta \begin{pmatrix} 0 & 0 & 0 \\ 0 & 0 & -1 \\ 0 & 1 & 0 \end{pmatrix} R_\varphi.$$

We can now derive the expression for a moving object as a composite function of its initial position and navigational data

$$(\dot{d}, \dot{\delta}) = (f_c \circ f_b \circ f_a)(d, \delta, V_r, \varphi, \theta, \psi, \dot{\varphi}, \dot{\theta}, \dot{\psi}) \quad (7)$$

where $(g \circ h)(\cdot) = g(h(\cdot))$ stands for a composite function.

IV. Kalman Filtering

A. State Equation

The state vector is composed of the sonar coordinates, i.e., $\boldsymbol{x} = (d \quad \delta)^T$. Considering the previous part and (7), the state equation can be written in the discrete domain according to the Euler method with a step number k

$$\boldsymbol{x_k} = f(\boldsymbol{x_{k-1}}, \boldsymbol{u_{k-1}}) + \boldsymbol{v_{k-1}} \quad (8)$$

where the input vector $\boldsymbol{u}_{k-1}$ is derived from navigational data such that $\boldsymbol{u}_{k-1} = (\boldsymbol{V}_r \quad \varphi \quad \theta \quad \psi \quad \dot{\varphi} \quad \dot{\theta} \quad \dot{\psi})_{k-1}^T$, $\boldsymbol{v_{k-1}}$ stands for the state noise vector whose covariance matrix is Q_{k-1} (explained in Section IV-C) and $f = f_c \circ f_b \circ f_a$ is a nonlinear state function determined in Section III.

B. Measurement Equation

The measurement vector $\boldsymbol{y} = (y^i \quad y^j)^T$ comprises obstacle coordinates on the screen in pixels, as determined by the detection step from Section VII-B. The measurement equation is then

$$\boldsymbol{y_k} = H_k \boldsymbol{x_k} + \boldsymbol{w_{k-1}} \quad (9)$$

where $\boldsymbol{w_{k-1}}$ stands for the measurement noise vector whose covariance matrix is R_{k-1} (see Section IV-C), and

$$H_k = H = \begin{pmatrix} \frac{1}{\Delta d} & 0 \\ 0 & \frac{1}{\Delta \delta} \end{pmatrix} \qquad \forall k$$

is the measurement matrix, where Δd (resp., $\Delta \delta$) stands for the along-track (resp., across-track) sampling rate in meters (resp., in degrees).

C. Covariance Matrices

For an optimal Kalman filtering, state and measurement noises as well as the initial state vector have to be Gaussian and mutually independent. However, the Kalman filter is known to be robust enough to work even in cases of noises that differ slightly from these hypotheses, in particular, for noises that are not exactly Gaussian.

The state variances were estimated by a heuristic procedure. The worst precision bounds of navigational parameters between the two AUVs are taken into account so as to simulate inputs of the state equation as uniformly distributed. Then, more than 8000 possible values of sonar coordinates were propagated in the process model, typically a range from 20 to 100 m by step of 1 m for d and a range from -0.5 to 0.5 rad by step of 0.01 rad for δ. This operation was repeated a hundred times and the average values stand as the estimated elements of the state covariance matrix, where state noises appear decoupled (actually with an absolute covariance less than 10^{-8})

$$Q_k = Q = 10^{-6}\begin{bmatrix} 0.48 & 0 \\ 0 & 0.024 \end{bmatrix} \qquad \forall k.$$

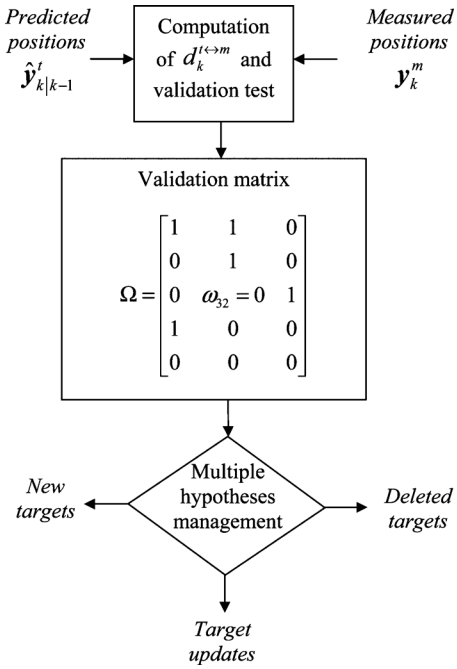

Fig. 2. Principle of data association procedure: example in the case of $M = 5$ and $T = 3$.

We assume that the measurement accuracy is about d_R meters in both the along-track and across-track directions. The measurement noises are then modeled as decoupled Gaussian noises with a standard deviation given in pixels but equivalent to d_R meters, which leads to the following measurement covariance matrix by introducing the sonar parameters:

$$R_k = \begin{bmatrix} [\mathrm{int}(d_R/\Delta d)]^2 & 0 \\ 0 & \left[\mathrm{int}\left(d_R/\left(\Delta\delta\Delta d y_k^i\right)\right)\right]^2 \end{bmatrix}$$

where y_k^i stands for the first component of the measurement vector y_k such that $\Delta d y_k^i$ determines the distance between the sonar and the detected obstacle. The $\mathrm{int}()$ function returns the closest integer. This latter function is coherent with the measurement vector components that are the screen coordinates of the target and hence integer values.

In this paper, the possible values of d_R range from 2 to 15 m. On the one hand, a high value is better to track large obstacles such as a wreck to avoid multiple tracks simultaneously on this specific obstacle. On the other hand, a small value is necessary to properly distinguish two smaller obstacles within close proximity of each other. In other words, for smaller values of d_R, the probability of detection as well as the probability of false alarm is higher.

D. Initialization

A Kalman filter is initialized for each new detected target. To avoid several Kalman filters on the same target, detection points that are too close to each other are fused by averaging their coordinates. This vicinity is given by a gate defined by the uncertainties of the measurement covariance matrix. This point will be discussed again in Section V.

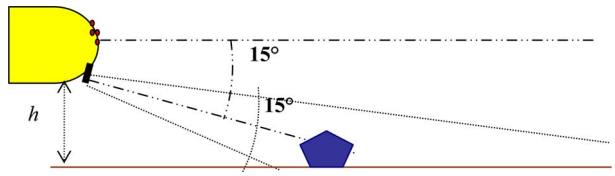

Fig. 3. Configuration of the *Reson Seabat 8101* FLS on *Redermor* AUV.

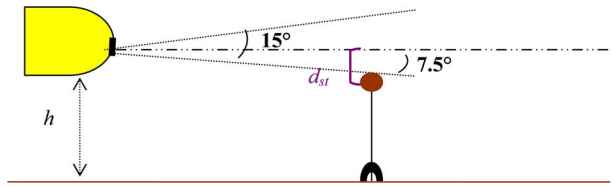

Fig. 4. Configuration of the *Blueview P450* FLS on *Daurade* AUV.

The initial state $\boldsymbol{x}_{0|0}$ consists of the sonar coordinates corresponding to the detected obstacle, i.e.,

$$\hat{\boldsymbol{x}}_{0|0} = \boldsymbol{x}_0 = (d_0 \quad \delta_0)^T = (y^i\Delta d \quad y^j\Delta\delta)^T$$

where y^i and y^j are the coordinates (in pixels) of the detected point on the screen for this obstacle.

To not be too confident in the first state, we set large uncertainties of about 5 m in range and 5° in azimuth. Indeed, these large values allow the Kalman filtering not to be too confident in the first measurement. Given the sonar parameters, we can derive the initial covariance matrix of

$$P_{0|0} = \begin{bmatrix} (100\Delta d)^2 & 0 \\ 0 & (3\Delta\delta)^2 \end{bmatrix}$$

for the *Reson Seabat 8101* FLS and

$$P_{0|0} = \begin{bmatrix} (30\Delta d)^2 & 0 \\ 0 & (30\Delta\delta)^2 \end{bmatrix}$$

for the *Blueview P450* FLS.

E. Prediction Stage

The prediction stage computes the new state $\hat{\boldsymbol{x}}_{k|k-1}$ given the previous one $\hat{\boldsymbol{x}}_{k-1|k-1}$, and is carried out by performing an unscented transform of $\hat{\boldsymbol{x}}_{k-1|k-1}$ because of the strong nonlinearity of the state function f. Details on the unscented Kalman filter can be found in [16]. The unscented transform is described hereafter.

We begin by creating a number of Sigma points $\boldsymbol{\chi}^i_{k-1|k-1}$, for $i = 1$ to $2n + 1$ with respective weight W_i, where n is the dimension of $\hat{\boldsymbol{x}}_{k-1|k-1}$. These points are uniformly distributed on an ellipsoid such that their mean and covariance are $\hat{\boldsymbol{x}}_{k-1|k-1}$ and $\boldsymbol{P}_{k-1|k-1}$ [17]. Practically, for $j \in \{1 \ldots n\}$, we compute

$$\boldsymbol{\chi}^0_{k-1|k-1} = \hat{\boldsymbol{x}}_{k-1|k-1}, \quad W_0 = \frac{\kappa}{n+\kappa}$$
$$\boldsymbol{\chi}^j_{k-1|k-1} = \hat{\boldsymbol{x}}_{k-1|k-1} + \left(\sqrt{(n+\kappa)P_{k-1|k-1}}\right)_j$$
$$W_j = \frac{1}{2(n+\kappa)}$$

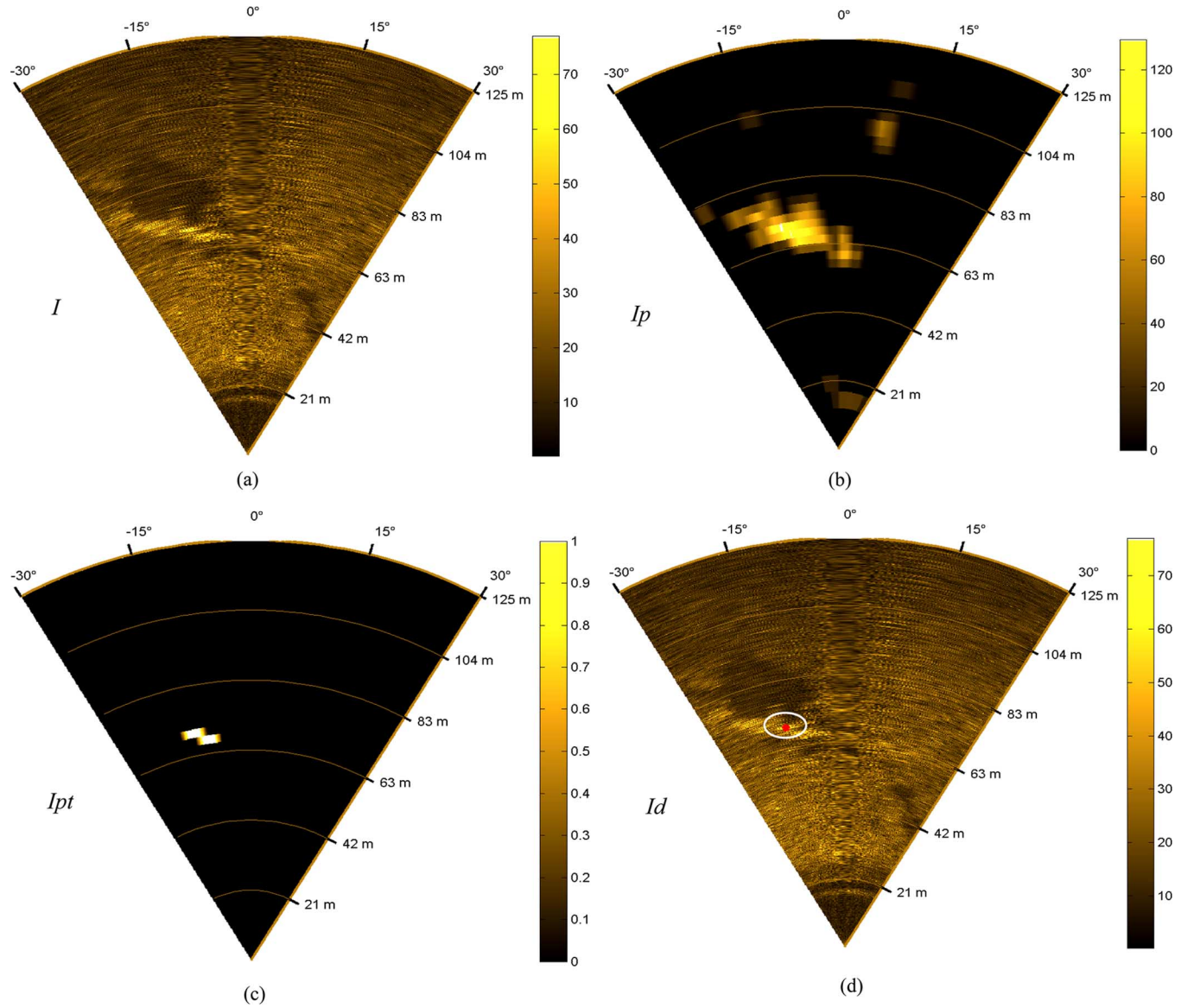

Fig. 5. Example of successive detection stages for a real sector-scan image (data of the 20th ping of the *Reson Seabat 8101* FLS sequence) where a shipwreck stands: (a) raw image *I*, (b) image *Ip* of detected areas, (c) thresholded image *Ipt*, (d) raw image *Id* with the final detected point in red (encircled in white).

$$\boldsymbol{\chi}^{j+n}_{k-1|k-1} = \hat{\boldsymbol{x}}_{k-1|k-1} - \left(\sqrt{(n+\kappa)P_{k-1|k-1}}\right)_j$$
$$W_{j+n} = \frac{1}{2(n+\kappa)}$$

where κ is usually set to $3-n$ [16] and $(\sqrt{(n+\kappa)P_{k-1/k-1}})_j$ stands for the jth column of the square root of the matrix $(n+\kappa)P_{k-1/k-1}$ obtained by a Cholesky decomposition [18].

Next, we compute the predicted values of these points given by the nonlinear function f

$$\boldsymbol{\chi}^{i}_{k|k-1} = f\left(\boldsymbol{\chi}^{i}_{k-1|k-1}, \boldsymbol{u}_{k-1}\right), \qquad \text{for } i = 1 \text{ to } 2n+1.$$

The predicted state can now be derived by the following weighted sum:

$$\hat{\boldsymbol{x}}_{k|k-1} = \sum_{i=0}^{2n} W_i \boldsymbol{\chi}^{\boldsymbol{i}}_{k|k-1}$$

as well as the associate covariance matrix

$$P_{k|k-1} = \sum_{i=0}^{2n} W_i \left[\chi^{i}_{k|k-1} - \hat{x}_{k|k-1}\right]\left[\chi^{i}_{k|k-1} - \hat{x}_{k|k-1}\right]^T.$$

F. Correction Stage

This final stage calculates the corrected sonar coordinates $\hat{\boldsymbol{x}}_{k|k}$ given the predicted one $\hat{\boldsymbol{x}}_{k|k-1}$ and the new measurement $\boldsymbol{y_k}$ which is a new detection at the kth filtering step. After computing $\hat{\boldsymbol{y}}_{k|k-1} = H\hat{\boldsymbol{x}}_{k|k-1}$ given the predicted state $\hat{\boldsymbol{x}}_{k|k-1}$, we can correct the state by applying the Kalman equations in the linear case

$$\begin{cases} \hat{\boldsymbol{x}}_{k|k} = \hat{\boldsymbol{x}}_{\boldsymbol{k}|\boldsymbol{k}-1} + K_k(\boldsymbol{y_k} - \hat{\boldsymbol{y}}_{\boldsymbol{k}|\boldsymbol{k}-1}) \\ K_k = P_{k|k-1}H_k^T\left(H_kP_{k|k-1}H_k^T + R_k\right)^{-1} \\ \quad = P_{k|k-1}H_k^T\left(R_k^v\right)^{-1} \\ P_{k|k} = P_{k|k-1} - K_kR_k^v(K_k)^T. \end{cases} \tag{10}$$

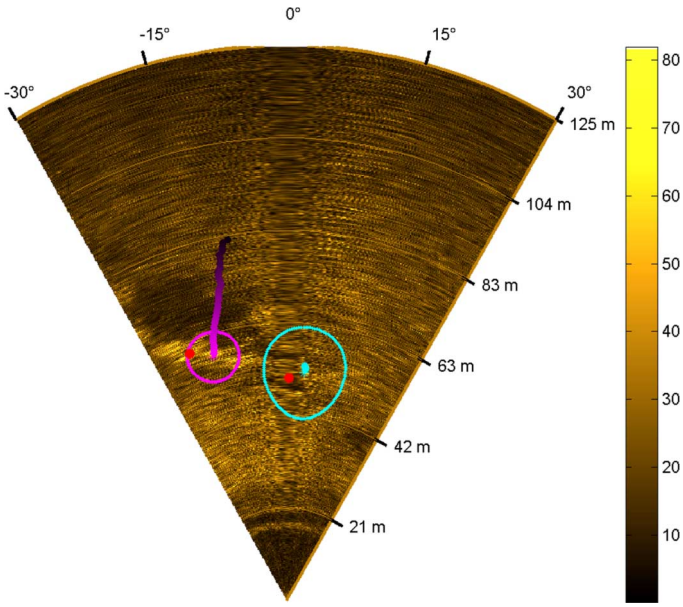

Fig. 6. Data of the 33rd ping of the *Reson Seabat 8101* FLS sequence: tracking of a shipwreck where $d_R = 15$ m: measurements in red, new filtered positions (at the center of the confidence ellipses) and trailing history of 32 previous positions in purple (vanishing colors for the oldest positions) and a new track with a large ellipse initialized by a false alarm in cyan.

The difference $\boldsymbol{v_k} = \boldsymbol{y_k} - \hat{\boldsymbol{y}}_{\boldsymbol{k}|\boldsymbol{k}-1}$ is called the innovation term and the associated covariance matrix is R_k^v. The impact of this term is controlled by the Kalman filter gain K_k.

If no detection occurs at this step, we keep the previous detection and the corresponding covariance matrix, i.e., $\boldsymbol{y_k} = \boldsymbol{y_{k-1}}$ and $R_k = R_{k-1}$. Another possibility would be to put large values in the diagonal matrix measurement R_k. However, this could lead to errors for the data association procedure described in the next section.

V. Data Association

Another crucial point of this multitarget tracking algorithm is the association of new measurements to existing tracks at each ping. Data association techniques can be divided into the following two categories [19]: 1) approaches that focus primarily on selecting target measurements that only fall within "validation gates" generated by existing tracks; or 2) approaches that focus on measurements and that try, for each of them, to find an existing track in their vicinity and create a new track if not.

The first approach is more suitable for tracking based on Kalman filtering that requires one or more measurements for use during the correction stage. This approach was chosen in [4] and [5], where data association was based on a nearest neighbor algorithm using the Euclidian distance between all the observations (i.e., measurements) and the predicted positions of tracked objects. As mentioned in [9], the global nearest neighbor method is indeed one of the simplest methods that can be used for data association. It also includes the formation of an observation-to-track assignment matrix to deal with conflict situations. In a similar way, we developed a process guided by previous works such as [20] and [21]. This process consists of two stages: first, we compute a validation matrix to visualize all possible matches between observations and existing tracks, and

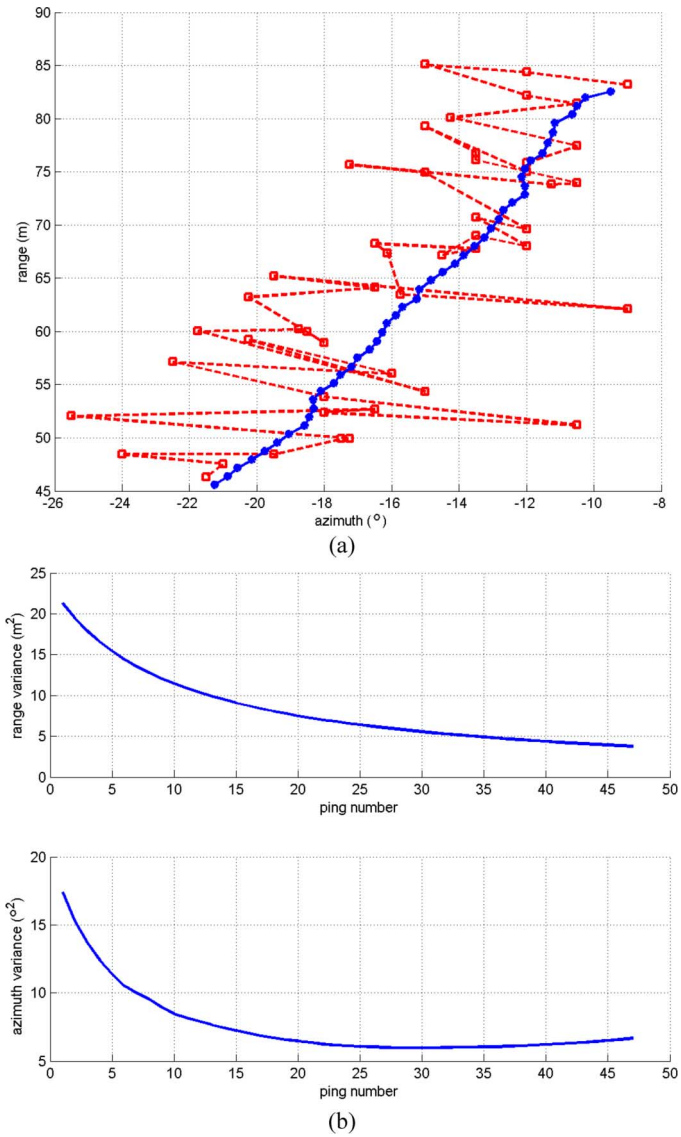

Fig. 7. (a) Filtering results on shipwreck sequence (dashed red line: measurements; blue line: estimated trajectory). (b) *A posteriori* variances evolution along the sequence.

then, we perform multiple-hypotheses management to decide on the final associations. Fig. 2 gives a diagram of the overall process.

In the first stage, for a given step $k > 0$, we need to deal with T existing tracks and M measurements. The validation matrix Ω of size $M \times T$ is defined with binary elements ω_{mt} to indicate if measurement $m \in \{1, \ldots, M\}$ lies in the validation gate for the target $t \in \{1, \ldots, T\}$. A validation gate is an ellipse centered on the predicted position $\hat{\boldsymbol{y}}_{k|k-1}^t$ whose axes are defined by the diagonal elements of the covariance matrix R_k^v of the innovation term $\boldsymbol{v}_k = \boldsymbol{y}_k^m - \hat{\boldsymbol{y}}_{k|k-1}^t$ (assumed to be normally distributed with zero mean). The Mahalanobis distance $d_k^{t \leftrightarrow m} = \boldsymbol{v}_k^T (R_k^v)^{-1} \boldsymbol{v}_k$ has a χ^2 distribution with r (equal to the number of components of the vector $\boldsymbol{y}_k$) degrees of freedom. Let χ_r^2 be the χ^2 variable with r degrees of freedom and $\chi_{r,1-\alpha}^2$ the critical value of this variable (tabulated) at a level of significance α. The second stage performs a validation test as follows: we accept the measurement at step k if $d_k^{t \leftrightarrow m} \leq \chi_{r,1-\alpha}^2$ where

$\chi^2_{r,1-\alpha} = 5.991$ for $r = 2$ and a significance level $\alpha = 0.05$ [22]. This validation test based on statistical properties of the innovation term of the Kalman filter was preferred to a matching function found in [1]. This matching function to be minimized is designed to check possible matches between new detections and existing tracks and takes into account Euclidian distances between elements being matched and their covariances.

The management of multiple hypotheses consists in deciding if a given track has to be initialized, can be updated, or has to be deleted. Of course, a measurement can be associated to only one target.

For a given track, i.e., for a column of the validation matrix, this decision depends on the number of binary elements set to one, and can be one of four cases.

1) If there is only one binary element set to one, the corresponding measurement is associated to this track for the correction stage of the Kalman filtering (if this is really the closest possible track).
2) If there are more than one binary elements set to one, we first consider the closest measurement $m_{\min}$ (the lowest corresponding distance $d_k^{t\leftrightarrow m_{\min}}$) and a validate gate defined by the uncertainties of the measurement covariance matrix. If other measurements "fall" in the ellipse, the effective measurement is the average of these measurements.
1) If no binary element is set to one, a copy of the previous measurement and of the corresponding covariance matrix is used for the correction stage.
2) Finally, for a row of the validation matrix with only zeros, a new track is created and a Kalman filter initialized.

Another point concerns track interruption. Hypothesis tests, like the Wald sequential probability ratio test or statistical tests of Mehra and Peschon, appear interesting because they are based on the innovation values [9], [23]. Unfortunately these tests were unusable here because of the difficulty in determining appropriate parameter values for the first one and because of lack of statistical samples (available innovation values) for the others. For these reasons, we chose a much simpler rule, besides the one used by Cobb *et al.*, which states that if no measurement is associated to a given track in three successive pings, then that track is interrupted [2].

VI. Case of an Obstacle in the AUV Path

In the previously developed method, the obstacle is assumed to be lying on the seafloor. However, the case of an obstacle that is in the water column, such as a tethered mine, also has to be considered. In this case, the Kalman filtering leads to a biased estimation of successive positions of the floating target. Indeed it will appear to be moving faster than the predicted positions according to the process model. Starting with this observation, a new algorithm is proposed that allows a deferred estimation of the z-coordinate (along the absolute z-axis) of the obstacle related to the vehicle using the information given by successive pings. This piece of information is of particular interest for obstacle avoidance but generally unavailable because of little or no sampling of the sonar data along the vertical axis for typical FLS with a single linear or cylindrical array. The only alternative is to use a more expensive and more complex sonar system (an interferometric sonar, a steerable sonar system, or a 3-D sonar system), which should commonly be avoided for the obstacle avoidance task of the AUV [24].

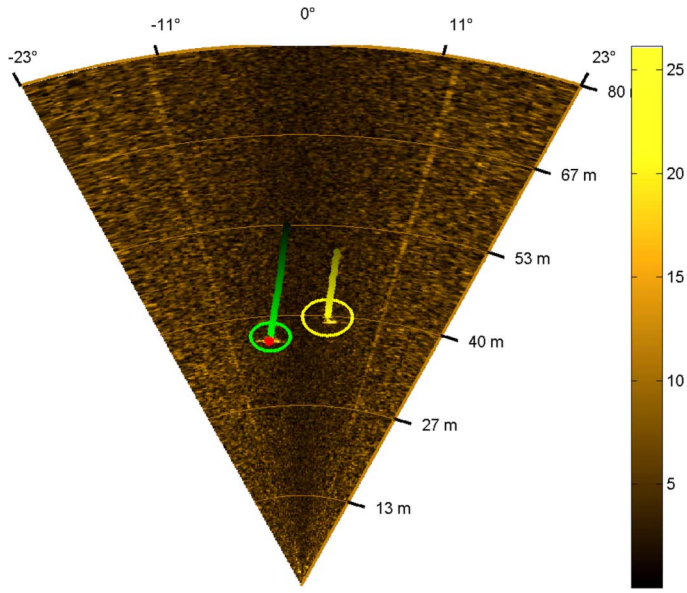

Fig. 8. Data of the 32nd ping of the first *Blueview P450* FLS sequence: tracking of two fake tethered mines in sight where $d_R = 2$ m: measurements in red, new filtered positions (at the center of the confidence ellipses) and trailing history of 31 previous positions in green (the steel mine) and of 19 previous positions in yellow (the rubber mine).

An estimation of the z-coordinate of the obstacle can be achieved by minimizing, at each step of the sequence, the root mean squared deviation (RMSD) between measured sonar positions (deduced from measurements $\boldsymbol{y_k}$) and predicted positions given by a new process model derived from the previous one with an additional parameter related to the z -coordinate. These predicted points only depend on the first measurement $\boldsymbol{y}_0$ and successive predicted displacements according to vehicle motion and assumed obstacle altitude.

This new model is achieved by modifying the third equation of (2) to put the distance $d_{\rm st}$ in meters between the sonar and the target along the z-axis in the world reference frame in the place of the altitude h of the sonar (as seen in Fig. 4). This leads to

$$-\sin(\theta)m_r^x + \cos(\theta)\sin(\varphi)m_r^y + \cos(\theta)\cos(\varphi)m_r^z = d_{\rm st} \tag{11}$$

and the previous f function becomes a new function $\tilde{f}$. For different possible values of $d_{\rm st} \geq 0$, we compute all of the predicted positions as follows.

- In the first step, the predicted sonar position is computed by taking into account the first measurement $\boldsymbol{y}_0$ such that $\tilde{\boldsymbol{x}}_0 = \breve{H}\ \boldsymbol{y}_0$ where $[\breve{H}] = \begin{bmatrix} \Delta d & 0 \\ 0 & \Delta\delta \end{bmatrix}$.
- For steps k greater than 0, we compute predicted sonar positions $\tilde{\boldsymbol{x}}_{\boldsymbol{k}} = \tilde{f}(\tilde{\boldsymbol{x}}_{\boldsymbol{k}-1}, \boldsymbol{u}_{\boldsymbol{k}-1}, d_{\rm st})$ given the previous one $\tilde{x}_{k-1}$.

Finally, we estimate the distance from the sonar to the target as

$$\hat{d}_{\rm st} = \underset{d_{\rm st}\in[0,1.2\times h]}{\arg\min} \sqrt{\sum_{k=0}^{N} \|\boldsymbol{x}_{\boldsymbol{k}} - \tilde{\boldsymbol{x}}_{\boldsymbol{k}}(d_{\rm st})\|^2/(N+1)}$$

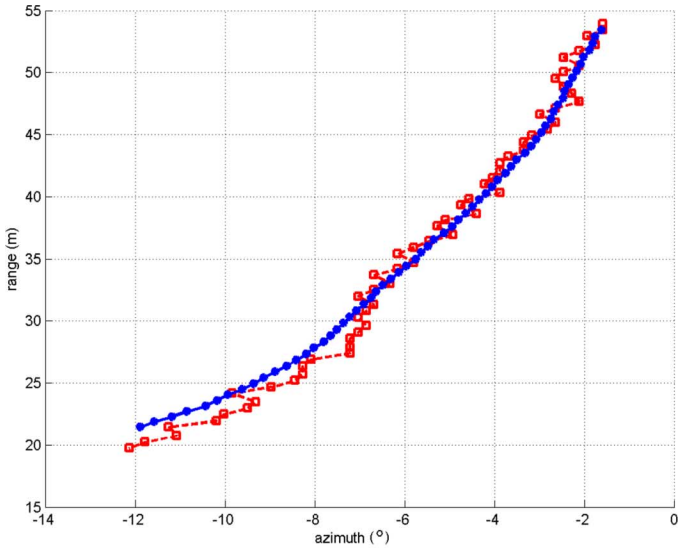

(a)

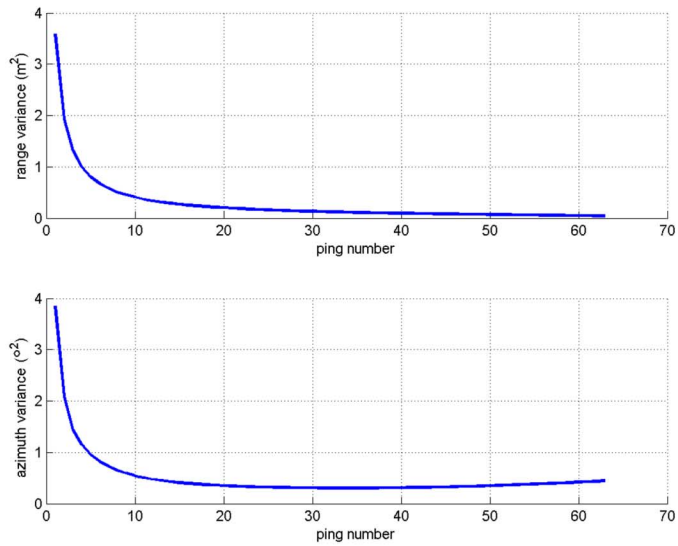

(b)

Fig. 9. (a) Filtering results for the longer track on the first *Blueview P450* FLS sequence (dashed red line: measurements; blue line: estimated trajectory). (b) *A posteriori* variances evolution along the sequence.

where $N+1$ is the number of pings used, $\boldsymbol{x_k} = \breve{H}\ \boldsymbol{y_k}$, and h is the altitude of the sonar at the first ping used. If the obstacle is below the vehicle, the maximum possible value of the distance from the sonar to the target is theoretically equal to the altitude of the sonar (case of a bottom object), but to prevent a wrong measured value, we choose a larger value, i.e., $1.2h$. If the object is not below but above the vehicle, this value is large enough to be considered as a safe distance.

Note that $\boldsymbol{x_k} - \tilde{\boldsymbol{x}}_{\boldsymbol{k}} = \breve{H}\ (\boldsymbol{y_k} - \tilde{\boldsymbol{y}}_{\boldsymbol{k}}) = \breve{H}\ \tilde{\boldsymbol{v}}_{\boldsymbol{k}}$, therefore we can say that the estimation consists in finding $\hat{d}_{\mathrm{st}}$ that minimizes the new innovation term $\tilde{\boldsymbol{v}}_{\boldsymbol{k}}$.

Here the RMSD is computed from two sets of polar coordinates whose components are not comparable as such. As a consequence, to make the RMSD similar to a distance measure between the two tracks, the azimuth component of sonar positions has to be multiplied by the corresponding range component so as to have the arc length instead.

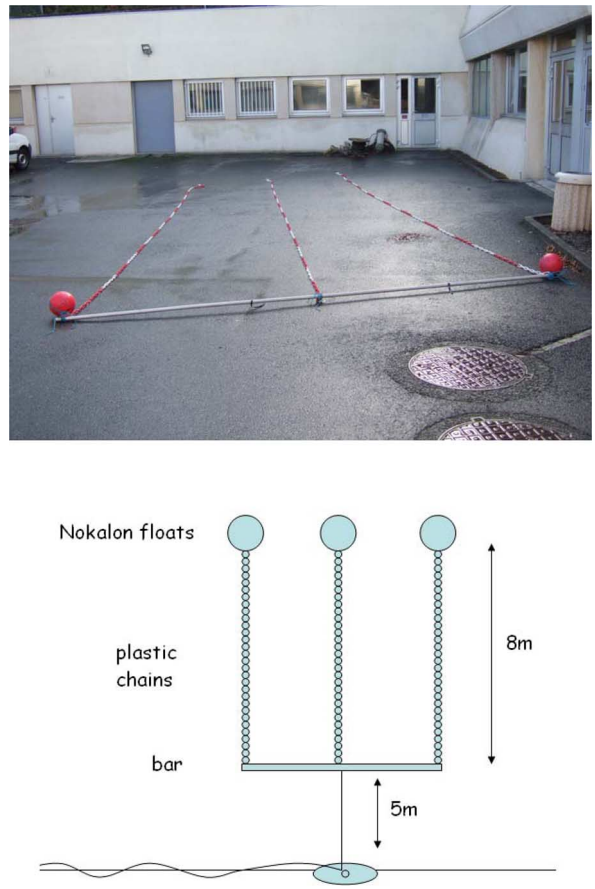

Fig. 10. Obstacle of the third sequence: a large thin obstacle made of a bar supporting chains and floats.

VII. Experimental Results

A. Data Description

1) Obstacle Avoidance Sonar Data:

a) Redermor AUV: The *Redermor* vehicle is an experimental platform developed by the GESMA (Groupe d'Etudes Sous-Marines de l'Atlantique). In its last release, the vehicle is equipped with an obstacle avoidance sensor that consists of a 240-kHz *Reson Seabat 8101* FLS [25]. The system can obtain a beamformed image over a 15° (vertical) × 60° (horizontal) sector with an across-track sampling rate $\Delta\delta$ equal to 1.5° and an along-track sampling rate Δd equal to 0.05 m. The sonar has been oriented 15° down from the horizontal plane (shown in Fig. 3).

To test the capability of the *Redermor* vehicle to react when obstacles are encountered on its way, GESMA organized experimental trials in April 2006 in Douarnenez Bay, France, named DETection et EVITement d'OBStacles (DEVITOBS).

b) Daurade AUV: The *Daurade* vehicle is a multipurpose experimental AUV for rapid environment assessment (REA) applications. It has been developed in the context of a project conducted by the Service Hydrographique et Océanographique de la Marine (SHOM) in cooperation with GESMA. The obstacle avoidance system is a *Blueview P450* FLS [26]. The system can obtain a beamformed image over a 15° (vertical) × 45° (horizontal) sector with an across-track sampling rate $\Delta\delta$ equal to 0.18° and an along-track sampling rate Δd equal to 0.17 m. The sensor looks straight ahead (see Fig. 4).

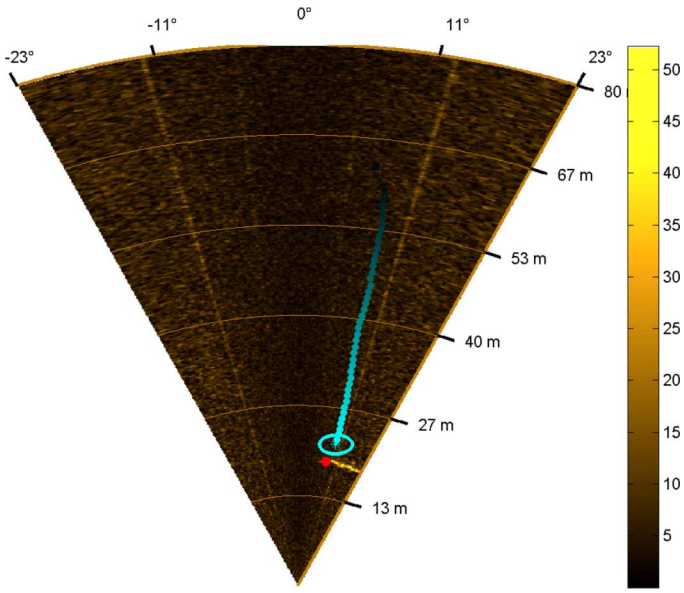

Fig. 11. Data of the 46th ping of the second *Blueview P450* FLS sequence: tracking of a large floating obstacle where $d_R = 5$ m: measurement in red, new filtered position (at the center of the confidence ellipse) and trailing history of 45 previous positions in cyan.

Data used in this paper have been collected by GESMA during two different sea trials near Brest, France, in March 2009 and April 2010.

2) Navigational Data: The two previous vehicles are fitted with different navigation systems that give us the following information:

- the vehicle velocity in relation to the seafloor, i.e., $\boldsymbol{V}_r = (v_r^x \quad v_r^y \quad v_r^z)^T$;
- the vehicle orientation (roll, pitch, and yaw) and its acceleration in relation to the world reference frame, i.e., the Euler angles (φ, θ, ψ) and their derivatives;
- the latitude and longitude coordinates of the vehicle;
- the altitude h of the vehicle from seafloor and also its depth from sea surface.

a) Redermor AUV: The Redermor AUV equipped with the *Reson Seabat 8101* uses a dead reckoning algorithm to compute the geographical position of the vehicle. The bottom velocity was obtained by a 300-kHz RDI DVL, and the vehicle orientation in the world reference frame was delivered by the OCTANS Attitude and Heading Reference System from iXSea (France). The dead reckoning process is initialized with a Wide Area Augmentation System (WAAS) Global Positioning System (GPS) receiver position.

b) Daurade AUV: The *Daurade* AUV equipped with the *Blueview P450* is built by ECA Robotics (Toulon, France) and uses the iXSea PHINS Inertial Navigation System. The PHINS system is directly fed by other navigation sensors, namely, a 300-kHz RDI DVL, a Paroscientific Depth Sensor, and a WAAS GPS receiver, and computes geographical position and velocity of the vehicle using Kalman filtering.

B. Obstacle Detection

As explained in Section II, an obstacle leads to a disturbance of the local statistics of the sonar image. To localize it, the sonar

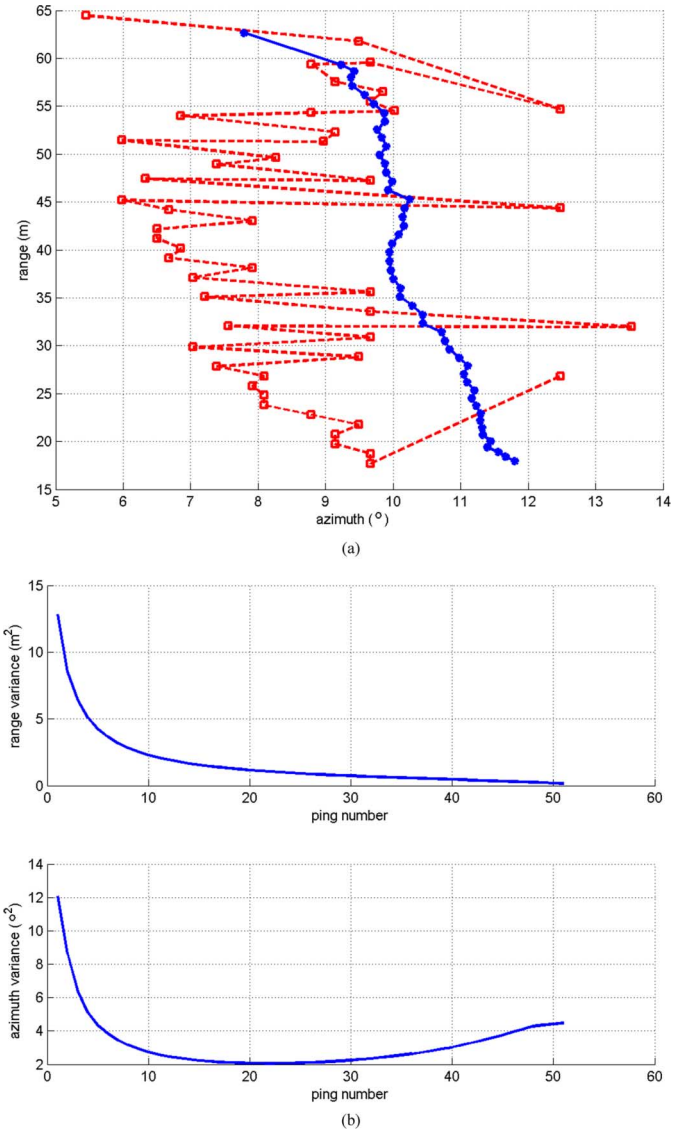

Fig. 12. (a) Filtering results on the second *Blueview P450* FLS sequence (dashed red line: measurements; blue line: estimated trajectory). (b) *A posteriori* variances evolution along the sequence.

image is first divided into snippets that consist of rectangular patches corresponding to an area of 5 m by 5 m with an overlap of 50%. For each snippet, we first compute the coefficient of variation c_v. For a Rayleigh-distributed variable, this ratio is constant and equal to 0.52 (see Section II) but this value can differ slightly for some systems like the *Reson Seabat 8101* FLS used in this paper, for which the revised ratio was estimated at 0.55. This difference can be explained by specific operational conditions that induce a better modeling of speckle by a Weibull law instead of a Rayleigh law [14]. Let c_v^{th} denote this theoretical value.

The test consists in comparing the local value of c_v to the theoretical value c_v^{th}. In other words, we consider that an object is present in the area if: $|c_v - c_v^{\text{th}}| > 0.1$. In that case of detection, the value of the pixels of the corresponding snippet is set to the mean pixel value (of the snippet). Otherwise, the pixels of the corresponding snippet are set to zero. By thresholding this image of overlapped snippets with a level of 80% of the maximum pixel value in this image, we can see areas of the image where pixels do not follow a Rayleigh distribution,

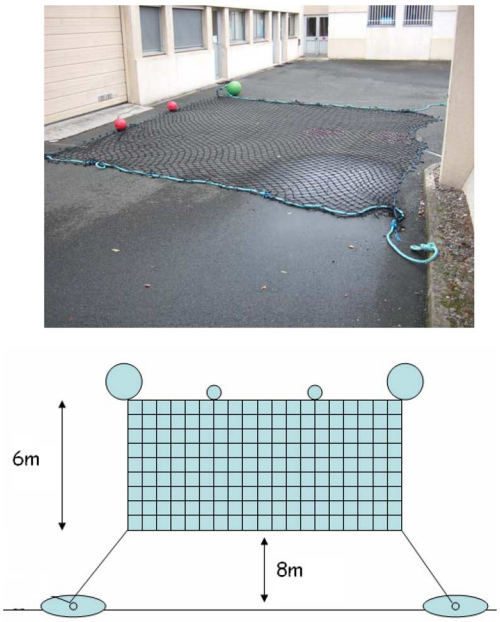

Fig. 13. Obstacle of the last sequence: a net with a large mesh.

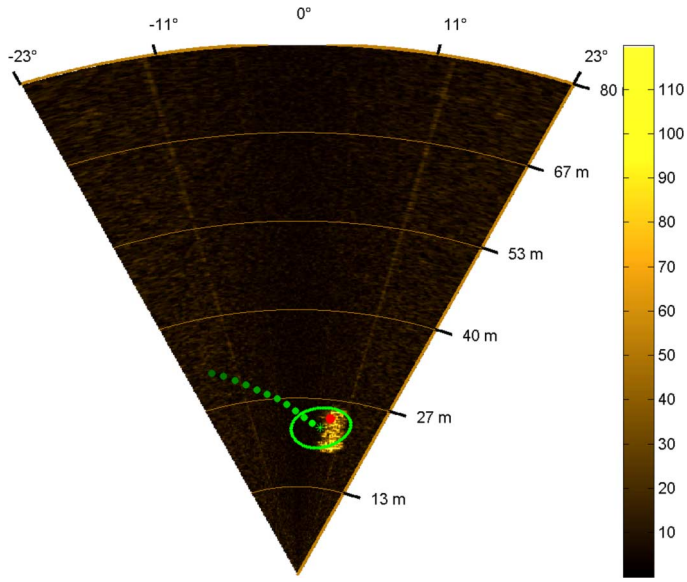

Fig. 14. Data of the 19th ping of the last *Blueview P450* FLS sequence: tracking of the net where $d_R = 2$ m: measurement in red, new filtered position (at the center of the confidence ellipse) and trailing history of 11 previous positions in green.

i.e., where an object has potentially been detected. The value of the previous threshold is a compromise between a lower value that would lead to an aggregation of detections and false alarms in the same area and a higher value that would result in lower detection rates and missing of faint objects. Last, for each of these detected areas, the pixel that had the maximum level in the original image is defined as the detection point (or measurement) and can initiate a Kalman filter. Fig. 5 gives an example of this process on a *Reson Seabat 8101* FLS image.

C. Ground Obstacle Avoidance

Figs. 6, 8, 11, and 14 are screenshots of a single ping where we can see one or two tracks with a trailing history from the previous filtered positions. Around the current predicted position, the 95% confidence ellipse that is a function of the diagonal elements of the state covariance matrix $P_{k/k}$ [27] is plotted. Whereas the target localization is more accurate, the length of the ellipse axes decreases; see Figs. 6, 8, 11, and 14 or videos dowloadable from www.ieeexplore.ieee.org for different sizes of ellipse. Also during an image sequence some tracks can be initiated but interrupted later and hence, are not visible on a single ping.

The first sequence was achieved by *Reson Seabat 8101* FLS where a shipwreck lies on the seafloor (see screenshot shown in Fig. 6, where a large echo area is followed by a large shadow area). As explained in Section IV-C, a large value fixed at 15 m for d_R is necessary to fuse all possible detected points relative to the same obstacle that is the large echo of the wreck. Because of that, a single track is initiated and updated with an average measurement. Fig. 7 shows a good filtering despite some noisy measurements at the end of the sequence. Variances, i.e., the diagonal elements of the state covariance matrix $P_{k/k}$, decrease monotonically toward a small value according to the accuracy of navigational data. Nevertheless, we can notice at the end a slight drawback for the azimuth variance that is probably due to a less accurate localization of the target in azimuth.

The second sequence is achieved by *Blueview P450* FLS where two fake tethered mines (see screenshot shown in Fig. 8) are in sight: a rubber one (yellow track in Fig. 8) was floating at about 15 m over the seafloor and had a diameter equal to 1 m (but probably smaller due to the pressure), another steel one (green track in Fig. 8) was floating at about 13 m and had a diameter equal to 0.75 m. These data were gathered in April 2010 near Brest, France. Sonar altitude was about 15 m above the seabed. The rubber mine is not tracked very far because of weaker echo level compared to the other. This is a consequence of the threshold based on the maximum level of the image of detected areas during the detection step (recall Section VII-B). The evolution of the variances is showed in Fig. 9(b). As the obstacle approaches (not visible at the step shown in Fig. 8, but can be seen in the corresponding downloadable video file), we can observe for this specific case of a tethered mine that Kalman filtering does not stop, however, it does underestimate the obstacle velocity. This is a consequence of the assumption of a ground obstacle. This case is discussed in Section VII-D.

The third sequence is also achieved by *Blueview P450* FLS where a large thin obstacle made of a bar supporting chains and floats is floating over the seafloor shown in the top part of Fig. 10. These data were gathered in March 2009, also near Brest, France. Sonar altitude was about 15 m above the seafloor. A track is shown in Fig. 11 with d_R of 5 m according to the size of the obstacle. A smaller value of d_R, such as 2 m for instance, would induce more than a single track on this obstacle. According to the complexity of this obstacle, it is impossible to know which part of it is detected at a given ping but, by considering the measurement variation in Fig. 12 (also visible in the video dowloadable from www.ieeexplore.ieee.org), it is clear that it is not always the same part. The evolution of the variances shown in Fig. 12 is approximately the same as that of the shipwreck sequence with a more difficult convergence for the azimuth prediction. As in previous cases, Kalman filtering underestimates the obstacle velocity.

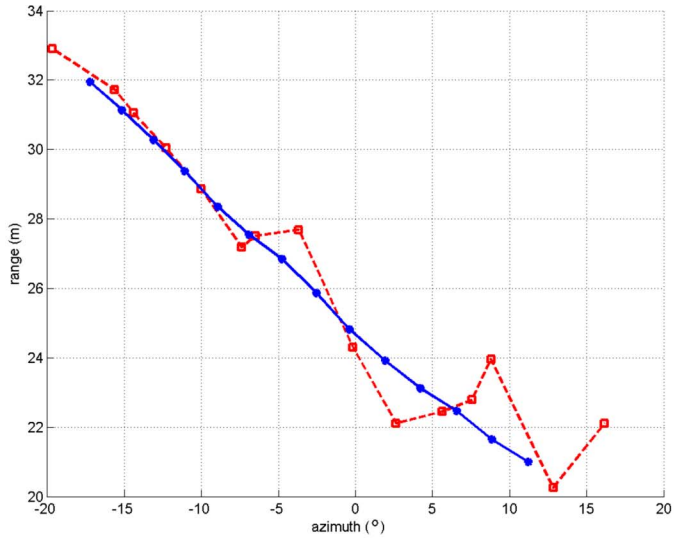

(a)

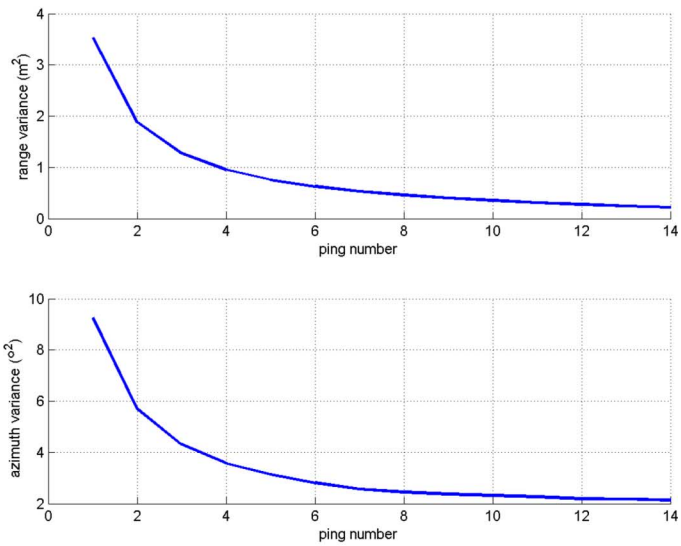

(b)

Fig. 15. (a) Filtering results on the last *Blueview P450* FLS sequence (dashed red line: measurements; blue line: estimated trajectory). (b) *A posteriori* variances evolution along the sequence.

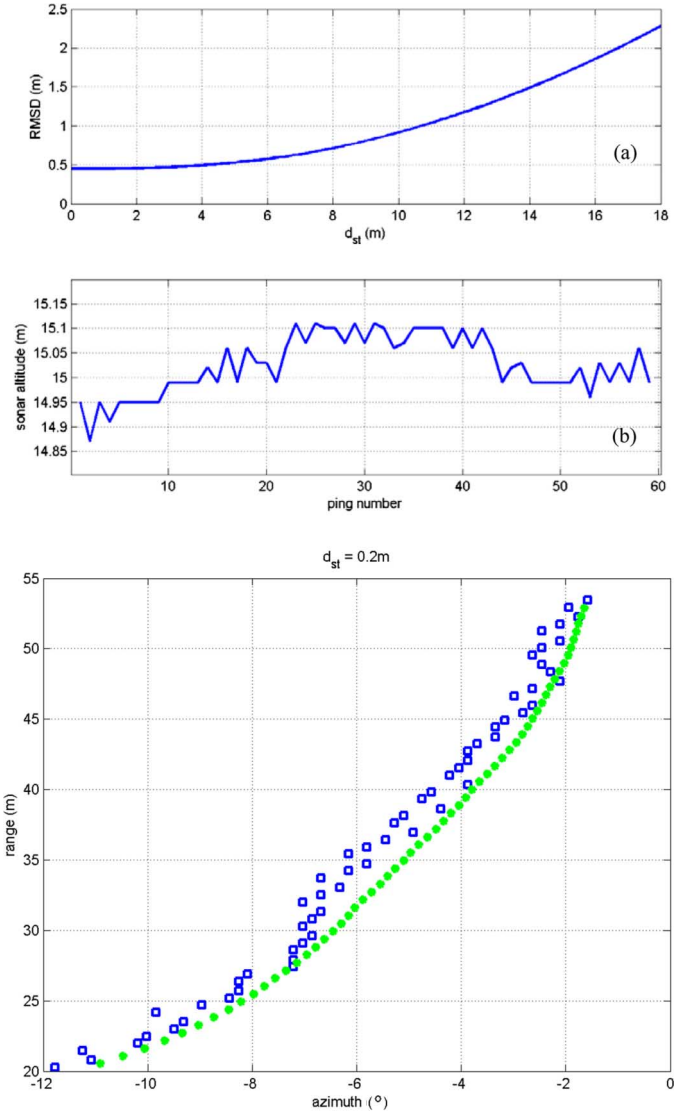

(c)

Fig. 16. Relative obstacle altitude estimation for track seen in Fig. 9: (a) RMSD versus $d_{\rm st}$; (b) sonar altitude versus ping number; (c) predicted points (green data points) and measurements (blue squared data points) for $d_{\rm st} = 0.2$ m.

The last sequence is obtained using the *Blueview P450* FLS, and shows images acquired along a turn of the vehicle, i.e., with large and fast attitude parameters variation. That is the reason that the obstacle is crossing from the left to the right of the screen. This obstacle, a net with a large mesh, is shown on Fig. 13. As was the case for the previous obstacle, these data were gathered in March 2009 near Brest, France. The track shown in Fig. 14 is obtained with d_R of 2 m. Both variances in Fig. 15 decrease monotonically, which proves a good performance of the Kalman filter even in this special case.

D. Relative Obstacle Altitude Estimation

In the following, we will call the experimental measurements as those given by the goodness-of-fit test described in Section II, and the manual measurements as those we estimated visually, i.e., by hand on each frame.

The *Daurade* sea trials in April 2010 were designed to assess the performance of the estimation method of the length of the tether of a moored mine proposed in Section VI. Two tethered spherical targets were deployed: a rubber one with a tether of 15 m and a steel one with a tether of 13 m. Fig. 16 shows the results concerning the second target. Fig. 16(a) and (b) shows a sonar altitude about 15 m and the RMSD minimization that gives an estimated distance $\hat{d}_{\rm st}$ of 0.2 m. That was approximately the case (expected value about 1.5 m): GESMA was testing avoidance capability in the case of an obstacle in the direction of travel of the vehicle. Predicted points given by the estimation method and experimental measurements points are plotted in Fig. 16(c) in case of $d_{\rm st} = 0.2$ m, that is to say, when these two sets of points are the closest to each other. In this case, as the target is punctual, the set of experimental measurements is very similar to the set of manual measurements, as shown in Fig. 17(a). That is why the estimation leads to the same estimated value for $d_{\rm st}$, whatever the set of measurements is.

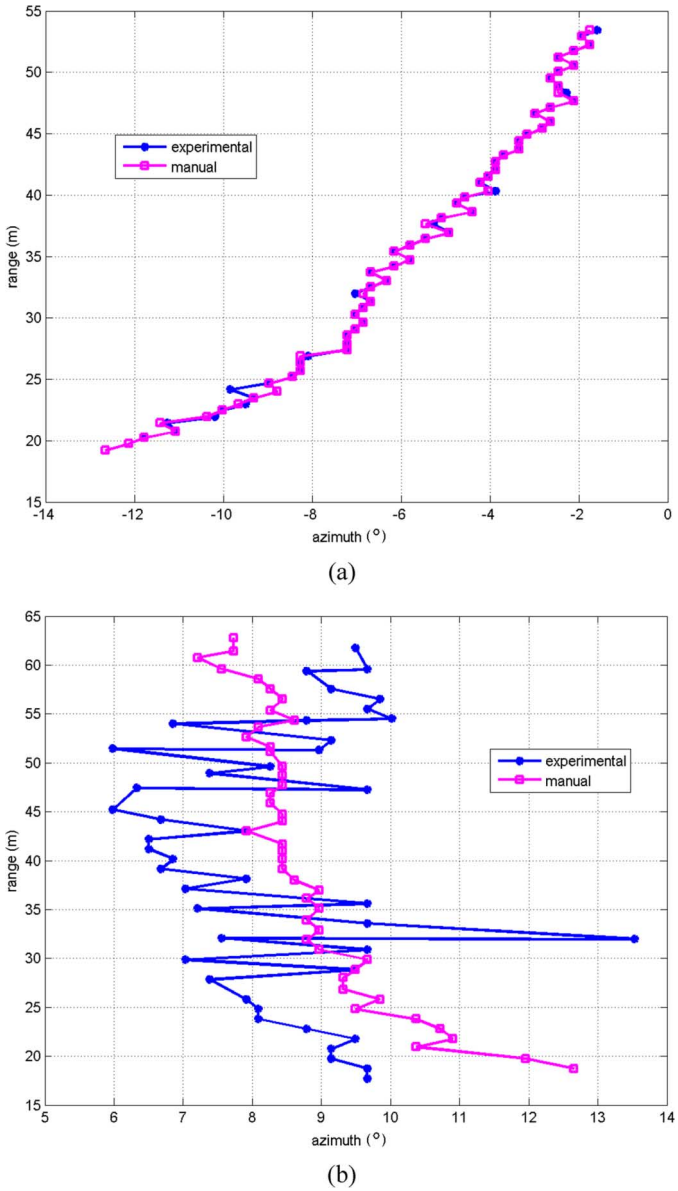

Fig. 17. Comparison between the set of experimental measurements (blue line) and the set of manual measurements (magenta line with squared data points) on *Blueview P450* FLS sequences: (a) data gathered in April 2010, (b) data gathered in March 2009.

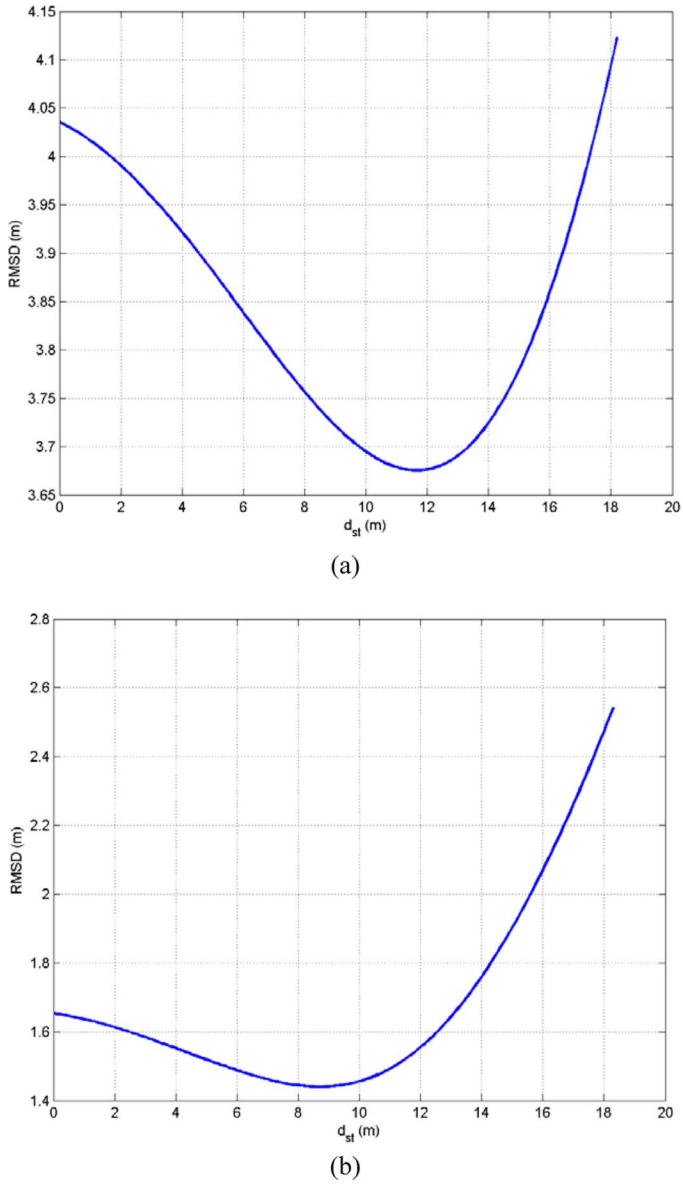

Fig. 18. Relative obstacle altitude estimation for track seen in Fig. 11: (a) RMSD versus d_{st} based on experimental measurements; (b) RMSD versus d_{st} based on manual measurements.

This task was more difficult for data gathered in March 2009 on a large obstacle seen in Fig. 10. Indeed, we can see in Fig. 18 that the estimated distance $\hat{d}_{\mathrm{st}}$ (11.7 m) based on experimental measurements differs from the one (8.7 m) based on manual measurements. This is probably due to noisy experimental measurements compared to manual measurements, as shown in Fig. 17(b). Moreover, as the three Nokalon floats are not clearly visible, we can assume that the obstacle was pushed down by current forces. Under this assumption, the detected echo area does not represent the Nokalon floats or the chains or the bar but probably a mix of them that leads to a value of 8.7 m between the obstacle and the sonar along the z-axis.

VIII. Conclusion

This paper has presented a framework for performing robust multitarget tracking, using navigational data. The main contribution of this work is the process modeling on which the Kalman filter is based. A Kalman filter is initialized every time a new target appears. The predicted position of the target is carried out by the state equation derived from the vehicle model and that takes navigational data as inputs. The nonlinearity of the state model was circumvented by performing an unscented transform. When a new measurement is available, it is put in the correction phase to adjust the target position. Multitarget tracking is achieved by a data association procedure that includes a validation test and a validation gate based on the innovation term of the Kalman filter. The robustness of the tracking has been shown on real data from two different FLSs as well as various obstacles. An interesting related contribution is the deferred estimation of the relative altitude of the obstacle based on the revised process model. This parameter is often an unavailable but important piece of information for obstacle avoidance purposes.

Future work will focus on obstacle characterization and classification. The objective is twofold: first, to discard benign obstacles such as a harmless school of fish, and second, to induce an appropriate avoidance maneuver. In addition, we aim to consider extending this work to the case of moving obstacles.

REFERENCES

[1] G. N. Williams, G. E. Lagace, and A. Woodfin, "A collision avoidance controller for autonomous underwater vehicles," in *Proc. IEEE Symp. Autonom. Underwater Veh. Technol.*, 1990, pp. 206–212.

[2] J. T. Cobb, B. Schulz, and G. Dobeck, "Forward-looking sonar target tracking and homing from a small AUV," in *Proc. MTS/IEEE OCEANS Conf.*, Washington, DC, Sep. 17–23, 2005, DOI: 10.1109/OCEANS.2005.1639948.

[3] D. M. Lane, M. J. Chantler, and D. Y. Dai, "Robust tracking of multiple objects in sector-scan sonar image sequences using optical flow motion estimation," *IEEE J. Ocean. Eng.*, vol. 23, no. 1, pp. 31–46, Jan. 1998.

[4] E. Trucco, Y. R. Petillot, I. T. Ruiz, K. Plakas, and D. M. Lane, "Feature tracking in video and sonar subsea sequences with applications," *Comput. Vis. Image Understand.*, vol. 79, pp. 92–122, 2000.

[5] Y. Petillot, I. T. Ruiz, and D. M. Lane, "Underwater vehicle obstacle avoidance and path planning using a multi-beam forward looking sonar," *IEEE J. Ocean. Eng.*, vol. 26, no. 2, pp. 240–251, Apr. 2001.

[6] D. Clark, I. T. Ruiz, Y. Petillot, and J. Bell, "Particle PHD filter multiple target tracking in sonar image," *IEEE Trans. Aerosp. Electron. Syst.*, vol. 43, no. 1, pp. 409–416, Jan. 2007.

[7] R. Mahler, "Multitarget Bayes filtering via first-order multitarget moments," *IEEE Trans. Aerosp. Electron. Syst.*, vol. 39, no. 4, pp. 1152–1178, Oct. 2003.

[8] N. O. Handegard and K. Williams, "Automated tracking of fish in trawls using the DIDSON (Dual frequency Identification SONar)," *ICES J. Mar. Sci.*, vol. 65, pp. 636–644, 2008.

[9] S. S. Blackman and R. Popoli, *Design and Analysis of Modern Tracking Systems*. Reading, MA: Artech House, 1999, ch. 6 and 13.

[10] L. Henriksen, "Real-time underwater object detection based on an electrically scanned high-resolution sonar," in *Proc. Symp. Autonom. Underwater Veh. Technol.*, Cambridge, MA, Jul. 19–20, 1994, pp. 99–104.

[11] J. S. Lee, "Statistical modeling and suppression of speckle in synthetic aperture radar images," in *Proc. Int. Geophys. Remote Sens. Symp.*, Ann Arbor, MI, May 18–21, 1987, pp. 1331–1339.

[12] F. Schmitt, L. Bonnaud, and C. Collet, "Contrast control for sonar pictures," *Proc. SPIE—Signal Image Process.*, vol. 2847, pp. 70–82, Aug. 1996.

[13] R. Caulcutt, *Statistics in Research and Development*. London, U.K.: Chapman & Hall, 1991, p. 19.

[14] F. Maussang, "Traitement d'images et fusion de données pour la détection d'objets enfouis en acoustique sous-marine," Thèse, de l'Université Joseph Fourier—Grenoble 1, Grenoble, France, Nov. 2005.

[15] I. Quidu, Y. Dupas, and L. Jaulin, "Theoretical optical flow for target position prediction on FLS images," in *Proc. Underwater Acoust. Meas. Conf.*, Nafplion, Greece, Jun. 21–26, 2009 [Online]. Available: http://www.uam-conferences.org/index.php/past-proceedings

[16] S. J. Julier and J. K. Uhlmann, "A new extension of the Kalman filter to nonlinear systems," in *Proc. 11th Int. Symp. Aerosp./Defense Sens. Simul. Controls*, 1997, Multi Sensor Fusion, Tracking and Resource Management II, pp. 182–193.

[17] R. Van Der Merwe and E. Wan, "Sigma-point Kalman filter for probabilistic inference in dynamic state-space models," in *Proc. Workshop Adv. Mach. Learn.*, Montreal, QC, Canada, Jun. 2003 [Online]. Available: http://cslu.cse.ogi.edu/publications/ps/merwe03a.ps.gz

[18] W. H. Press, S. A. Teukolsky, W. T. Vetterling, and B. P. Flannery, *Numerical Recipes in C: The Art of Scientific Computing*, 2nd ed. Cambridge, U.K.: Cambridge Univ. Press, 1992, p. 350.

[19] Y. Bar-Shalom and T. E. Fortmann, "Mathematics in science and engineering," in *Tracking and Data Association*. San Diego, CA: Academic, 1988, vol. 179, ch. 1.

[20] T. E. Fortmann, Y. Bar-Shalom, and M. Scheffe, "Sonar tracking of multiple targets using joint probabilistic data association," *IEEE J. Ocean. Eng.*, vol. OE-8, no. 3, pp. 173–184, Jul. 1983.

[21] B. Jida, R. Lherbier, M. Wahl, and D. Hamad, "Détection automatique dans les données télémétriques et association spatio-temporelle par réseaux bayésiens—Application au suivi de véhicules," presented at the MajecSTIC Conf., Lorient, France, Nov. 22–24, 2006.

[22] Y. Bar-Shalom and E. Tse, "Tracking in a cluttered environment with probabilistic data association," *Automatica*, vol. 11, pp. 451–460, 1975.

[23] R. K. Mehra and J. Peschon, "An innovations approach to fault detection and diagnosis in dynamic systems," *Automatica*, vol. 7, pp. 637–640, 1971.

[24] C. D. Loggins, "A comparison of forward-looking sonar design alternatives," in *Proc. MTS/IEEE OCEANS Conf.*, Honolulu, HI, 2001, pp. 1536–1545.

[25] Reson, "SeaBat," [Online]. Available: www.reson.com/products/seabat/

[26] BlueView Technologies, "2D multibeam imaging sonar," [Online]. Available: www.blueview.com/2d-Imaging-Sonar.html

[27] N. R. Draper and H. Smith, *Applied Regression Analysis*, 2nd ed. New York: Wiley, 1981, pp. 108–109, ISBN: 0471029955.

Isabelle Quidu was born in Pontivy, France, in 1974. She received the Ph.D. degree in electronics from the University de Bretagne Occidentale, Brest, France, in 2001.

From 2002 to 2005, she was a Research Engineer at Thales Underwater Systems in the field of mine warfare. Since 2005, she has been an Associate Professor at the Ecole Nationale Supérieure de Techniques Avancées (ENSTA) Bretagne (formerly ENSIETA), Brest, France, and a member of the Ocean Sensing and Mapping (OSM) team. She is also a member of Lab-STICC UMR CNRS 6285. Her research interests are in detection and classification of underwater targets in sonar images.

Luc Jaulin was born in Nevers, France, in 1967. He received the Ph.D. degree in automatic control from the University of Orsay, Orsay, France, in 1993.

He has been a Professor of Robotics at the Ecole Nationale Supérieure de Techniques Avancées (ENSTA) Bretagne, Brest, France, since 2004. He is part of the Ocean Sensing and Mapping (OSM) team and his research is in underwater robotics using interval methods and constraint propagation. He is a member of Lab-STICC UMR CNRS 6285.

Alain Bertholom was born in Quimper, France, in 1971. He graduated in electronics from the French Department of Defense in 1993.

He joined the Naval Robotics Department, Groupe d'Etudes Sous-Marines de l'Atlantique (GESMA), Brest, France, in 1998. He was involved in real-time embedded software development and sea trials for the *Redermor I* and *II* autonomous underwater vehicles (AUVs). He also worked on navigation purposes. Since September 2009, he has been the Technical Manager of the Covert REA *Daurade* AUV.

Yann Dupas was born in Montereau, France, in 1981. After finishing his first studies at the Autun Military College, Autun, France, he became a military student at the the Ecole Nationale Supérieure de Techniques Avancées (ENSTA) Bretagne, Brest, France, in September 2001.

He became a Military Engineer in September 2005. He joined the Naval Robotics Department, Groupe d'Etudes Sous-Marines de l'Atlantique (GESMA), Brest, France, and started working on obstacle detection and avoidance for autonomous underwater vehicles (AUVs), mission planification, and sea trials organization with the GESMA AUV *Redermor II*. In 2008, he became a Technical Manager for the new REA project and achieved acquisition of the new covert REA AUV *Daurade*. In September 2009, he became a Project Manager for the covert REA project at the Service Hydrographique et Océanographique de la Marine (SHOM), Brest, France.